Since January 2020 Elsevier has created a COVID-19 resource centre with free information in English and Mandarin on the novel coronavirus COVID-19. The COVID-19 resource centre is hosted on Elsevier Connect, the company's public news and information website.

Journal of Organometallic Chemistry 914 (2020) 121219

Contents lists available at ScienceDirect

Journal of Organometallic Chemistry

journal homepage: www.elsevier.com/locate/jorganchem

Anticancer activity studies of novel metal complexes of ligands derived from polycyclic aromatic compound *via* greener route

Mahantesh Kumbar [a], Sangamesh A. Patil [a, *], Shivakumar S. Toragalmath [b], Shivashankar M. Kinnal [a], Arun Shettar [c], Joy H. Hosakeri [d]

[a] P. G. Department of Chemistry, Karnatak University, Dharwad, 580003, Karnataka, India
[b] K L E's, P. C. Jabin Science College, Autonomous, Vidyanagar, Hubballi, 580031, Karnataka, India
[c] P. G. Department of Biotechnology and Microbiology, Karnatak University, Dharwad, 580003, Karnataka, India
[d] Department of Biotechnology and Bioinformatics, Akkamahadevi Women's University, Vijayapura, 586108, Karnataka, India

ARTICLE INFO

Article history:
Received 20 January 2020
Received in revised form
2 March 2020
Accepted 6 March 2020
Available online 7 March 2020

Keywords:
Inorganic medicine
Green synthesis
DNA cleavage
Anticancer
Cytotoxicity
IC_{50}

ABSTRACT

Methoxy and *tert*-butyl substituted carboxamide, carboxylic acid and hydrazone Schiff base groups have been assembled into our newly designed fluorenone based ligands and prepared coordination compounds of some first row transition metals and characterized thoroughly with spectroscopic (^{1}H and ^{13}C NMR, IR, GC–MS, UV–Vis), analytical, TGA and molar conductance measurements. The stoichiometry of all the metal complexes is found to be 1: 2 (M: L_2) with the general formula, $[M(L)_2]$, where L is a singly deprotonated ligand and the geometry of all the metal complexes is found to be octahedral. Ligands and their metal complexes successfully cleaved the pBR322 plasmid DNA and in case of anticancer activity against MCF–7 (human breast adenocarcinoma) cell line, the synthesized compounds found to exhibit excellent activity with prominent apoptotic effect which is characterized by cell shrinkage, cell breakage and turgidity and results were compared with the standard drug cisplatin. Very significant anticancer activity was observed for compounds L^1H, $Cu(L^1)_2$, $Cu(L^2)_2$, $Ni(L^1)_2$ and $Ni(L^2)_2$ with IC_{50} value of <10 μgmL^{-1}. Molecular docking studies were performed to assess the bonding mode of synthesized compounds. In case of antioxidant activity study, the compounds L^1H, $Ni(L^1)_2$, $Ni(L^2)_2$, $Cu(L^1)_2$ and $Cu(L^2)_2$ exhibited significant scavenging activity with good percentage when compared with remaining tested compounds.

1. Introduction

Remedy for cancer is certainly one of the big medical challenges to the scientists of 21st century and is one of the current research hotspots. The escalating research to fight against cancer is getting us closer to a future, where cancer becomes a curable disease. As a researcher, we dream of curing cancer as easy as the deadly diseases *viz.*, chickenpox, smallpox, polio, measles, sars (severe acute respiratory syndrome), yellow fever, malaria etc., [1]. Although existing drugs show efficacy, their lack of selectivity for tumor cells over normal cells can lead to severe side effects [2]. Cancer is caused by mutations that transform healthy cells into tumor cells. Recent studies have demonstrated that, there will not be a match between tumors of two patients. It implies that, the scientists should work on medicines that are tailored to cure a specific patient. Platinum based drugs are actively used in treating various types of cancers; however, drug resistance, adverse side effects and low specificity are common in platinum chemotherapy [3,4]. To overcome these abnormalities to greater extent, in recent years other metal based drugs have been developed and tested for their anticancer efficacy [5]. Important ones are the coordination compounds of Ni(II), Cu(II), Zn(II) and Ru(II) which can overcome the limited activity of cisplatin and its analogous [6,7].

Our current research puts in effort to crack a new anticancer drug candidate which could prove to be a better medicine. In our present work, the hydrazone Schiff base ligands derived from 9-oxo-9*H*-fluorene-1-carboxylic acid and their respective Co(II), Cu(II) and Ni(II) complexes are synthesized impeccably and analyzed. Hydrazones play an important role in inorganic medicinal chemistry. They can easily form stable complexes with transition metal ions and can exhibit interesting photophysical and biological properties [8]. They exhibit biological activities such as

* Corresponding author.
E-mail address: patil1956@rediffmail.com (S.A. Patil).

https://doi.org/10.1016/j.jorganchem.2020.121219
0022-328X/

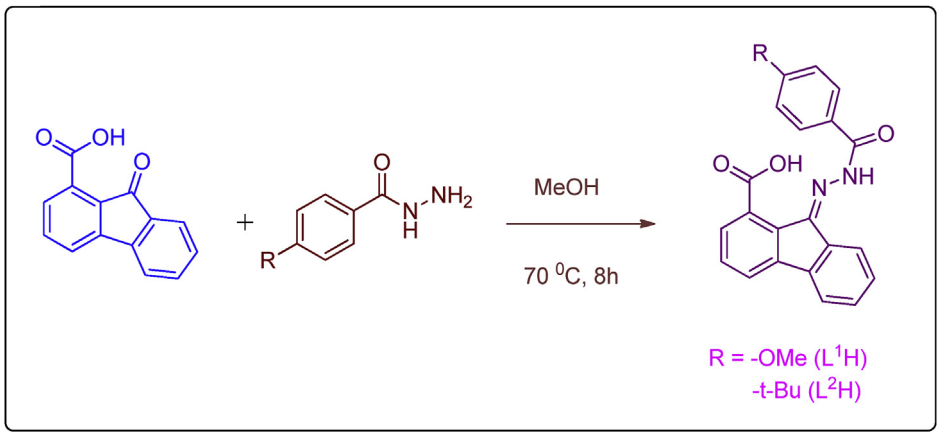

Scheme 1. Schematic route for the synthesis of hydrazone Schiff bases, L^1H and L^2H.

antibacterial [9], antioxidant [10], antifungal [11], antitubercular [12], anti-inflammatory [13] and anticancer [14].

Fluorenone is no doubt a polycyclic aromatic compound, one could doubt about its therapeutic property. But, the literature reveals that derivatives of fluorenone have exhibited interesting biological activities. Arylsulfonylspiro[fluorene-9,5′-imidazolidine]-2′,4′-diones are found to be effective as aldose reductase inhibitors [15]. Azabenzo[a]fluorene-5,6-diones have comparable cytotoxicities against cancer cell lines *in vitro*, with that of standard drug doxorubicin [16]. Our previous publication [17] have successfully established the anticancer efficacy of copper (II) complex of fluorenone based ligand; which exhibited better anticancer activity against human breast carcinoma (MCF−7) cell line when compared to that of standard drug paclitaxel.

These results prompted us to synthesize new ligands which are embedded with fluorenone moiety, carboxylic acid, carboxamide and hydrazone groups. The metal complexes are synthesized from these ligands *via* eco-friendly routes employing green solvents. The ligands and their respective metal complexes were tested for their anticancer activities with MTT assay against breast cancer (MCF−7) cell line, DNA cleavage study was performed using pBR322 plasmid DNA. Antioxidant activity study was carried out through DPPH free radical-scavenging ability assay. Molecular docking studies were also carried out to examine the bonding mode of synthesized compounds.

2. Experimental

2.1. Materials and physical methods

All the raw materials including reagents, catalysts, solvents and drying agents were of fine chemical grade and utilized as received by the vendor. The MTT [2-(4,5-dimethylthiazol-2-yl)-3,5-diphenyl-2*H*-tetrazol-3-ium bromide] dye was purchased from Sigma, St. Louis, MO, USA.

Infrared (IR) spectra of the synthesized materials were recorded in the range of 4000−550 cm^{-1} with *PerkinElmer Spectrum Two* FT−IR spectrometer. By using TMS as internal reference compound, ^1H and ^{13}C NMR spectra were recorded in DMSO-d_6 solvent on *JEOL* 400 MHz and *Bruker* 400 MHz spectrometer at room temperature. Using *ThermoQuest* Elemental Analyzer, elemental analyses of the compounds was carried out. Electronic spectra of ligands and their metal complexes were recorded on a *PerkinElmer LAMBDA 365* UV−Vis spectrophotometer in the range of 1100−200 nm. Thermal analysis of the metal complexes was carried out with an *SDT Q600* analyzer, by increasing the temperature from RT to 1000 °C at the rate of 10 °C min^{-1}. The molar conductance measurements were made on *ELICO CM 180* conductivity meter with a cell constant of 1.0 after calibration with standard KCl solution at 25 °C. LC−ESI−MS spectra were recorded on *LCMS 2010A, SHIMADZU* instrument.

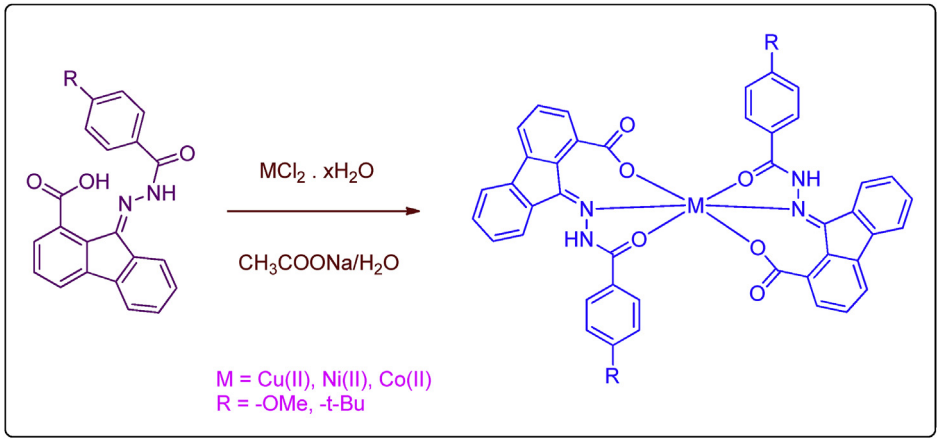

Scheme 2. Schematic route for the synthesis of transition metal complexes.

Table 1
Prominent infrared frequency (in cm^{-1}) of ligands (L^1H and L^2H) and their respective metal complexes.

Compound	$\nu(N-H)^{br}$	$\nu(C=O)^{s}$ Carboxylic acid	$\nu(C=O)^{s}$ Amide	$\nu(C=N)^{s}$	$\nu(COO)$		$\nu(O-H)^{br}$ Acidic	$\nu(M-O)^{m}$
					ν_{asym}	ν_{sym}		
L^1H	3407	1701	Masked	1668	1521	1359	2434	–
$Cu(L^1)_2$	3498	disappeared	1610	1628	1554	1374	disappeared	528
$Ni(L^1)_2$	3479	disappeared	1615	1631	1545	1378	disappeared	538
$Co(L^1)_2$	3426	disappeared	1621	1628	1544	1377	disappeared	532
L^2H	3325	1705	Masked	1680	1511	1317	2523	–
$Cu(L^2)_2$	3382	disappeared	1645	1623	1575	1381	disappeared	495
$Ni(L^2)_2$	3397	disappeared	1638	1637	1577	1370	disappeared	535
$Co(L^2)_2$	3376	disappeared	1640	1619	1578	1372	disappeared	540

m = medium, s = strong, br = broad.

2.2. Synthesis

2.2.1. Procedure for the synthesis of 9-oxo-9H-fluorene-1-carboxylic acid

9-Oxo-9*H*-fluorene-1-carboxylic acid is prepared from fluoranthene using potassium dichromate as an oxidizing agent as per the protocol reported in our previous publication [18]. Yield: 99%; Color: Orange; M. P. 194–196 °C (Lit. 196–198 °C).

2.2.2. General procedure for the synthesis of hydrazone Schiff base

An equimolar mixture of 9-oxo-9*H*-fluorene-1-carboxylic acid (2.5 g, 11.15 mmol) and benzohydrazides (4-methoxy and 4-*tert*-butyl derivatives) (11.15 mmol) is refluxed in 50 mL methanol at 70 °C for 8 h (Scheme 1) [19]. The contents are partially soluble at RT. About 30 min of heating at 70 °C, the reaction mixture turns orange to yellow and yellow solids separate, which indicates the formation of desired product. The reaction is monitored by TLC in 9:1 chloroform: methanol. The solids are filtered and washed with cold methanol and dried under *vacuum* at 40 °C. L^1H: Yield: 3.9 g; 94%. Color: Canary yellow. L^2H: Yield: 4.1 g; 92%. Color: Canary yellow.

2.2.3. General procedure for the synthesis of transition metal complexes

Copper (II) complex: The copper (II) complexes are synthesized in water at room temperature. Equimolar mixtures of ligand (500 mg, 1.33 mmol), copper (II) chloride (226 mg, 1.46 mmol) and sodium acetate (109 mg, 1.33 mmol) were stirred in 10 mL DI (deionized) water for 8 h at RT (Scheme 2). The solid separated is filtered, washed with water and dried under *vacuum* at 50 °C. $Cu(L^1)_2$: Yield: 518 mg, 48%; Color: Green. $Cu(L^2)_2$: Yield: 532 mg, 51%; Color: Apple green.

Nickel/Cobalt (II) complexes: The Co(II) and Ni(II) complexes are synthesized in water under reflux conditions. Equimolar mixtures of ligand (500 mg, 1.33 mmol), metal chloride ($CoCl_2.6H_2O$/$NiCl_2.6H_2O$) and sodium acetate (109 mg, 1.33 mmol) were refluxed in 10 mL DI water for 8 h. The solid separated is filtered, washed with water and dried under *vacuum* at 50 °C. $Co(L^1)_2$: Yield: 580 mg, 54%; Color: Yellow. $Co(L^2)_2$: Yield: 467 mg, 45%; Color: Tangerine. $Ni(L^1)_2$: Yield: 538 mg, 50%; Color: Golden yellow. $Ni(L^2)_2$: Yield: 497 mg, 48%; Color: Primrose yellow.

Table 2
Solution electronic absorption spectral data of ligands (L^1H and L^2H) and their copper (II) complexes.

Compound	λ_{max} in cm^{-1} (nm)	Band assignments	Geometry
L^1H	28,571 (350), 24,096 (415), 22,727 (440)	$\pi \rightarrow \pi^*$, $n \rightarrow \pi^*$, CT	–
$Cu(L^1)_2$	14,144 (707)	$^2T_{2g} \leftarrow {}^2E_g$	Octahedral
L^2H	28,735 (348), 24,390 (410), 22,935 (436)	$\pi \rightarrow \pi^*$, $n \rightarrow \pi^*$, CT	–
$Cu(L^2)_2$	13,947 (717)	$^2T_{2g} \leftarrow {}^2E_g$	Octahedral

3. Bioassay

3.1. Cytotoxicity: MTT cell proliferation assay

The effect of ligands and their metal complexes on the viability of breast cancer cells was determined using the standard colorimetric MTT [2-(4,5-dimethylthiazol-2-yl)-3,5-diphenyl-2*H*-tetrazol-3-ium bromide] assay [20]. The monolayer cell culture was trypsinized and the cell count was adjusted to 1.0×10^5 cellsmL^{-1} using DMEM (Dulbecco's Modified Eagle Medium) containing 10% FBS and seeded to 96-well microtiter plates (Falcon, Becton–Dickinson, Franklin Lakes, NJ, USA). After 24 h; of plating, cells were serum starved for 24 h. Respective concentrations (10, 20, 30, 40 and 50 μgmL^{-1}) of ligands and their metal complexes were added to serum free medium and the assay was terminated after 48 h. Medium was removed and 200 μL of DMSO was added and the amount of formazan formed was measured at 595 nm on a Model 680 microplate reader (Bio-Rad Laboratories, Inc., Hercules, CA, USA). The percentage growth inhibition was calculated using the following formula and concentration of test drug needed to inhibit cell growth by 50% (IC_{50}) is generated from the dose-response curves for each cell line. This assay is based on the reduction of MTT by the mitochondrial dehydrogenase of intact cells to a purple formazan product [21].

$$\text{Inhibition Percentage} = \text{OD of Test sample} \div \text{OD of control} \times 100$$

3.1.1. Statistical analysis

All experiments were performed in triplicates (n = 3) and the numerical data are presented as mean ± standard deviation (SD).

3.2. Photocleavage of pBR322 DNA

The DNA cleavage activity of the newly synthesized ligands and their metal complexes was monitored by Agarose gel electrophoresis on pBR322 DNA (200 ng) in TAE buffer (40 mM Tris-Acetate, 1 mM EDTA) to yield a total volume of 10 μL and then incubated in dark for 30 min at 37 °C. Different concentrations of compounds were tested; 10, 30, 50 and 100 μgmL^{-1}. The reaction was incubated at 37 °C for 2 h and 3 μL of loading buffer (bromophenol blue in H_2O) was added to each tube and the mixed samples were loaded on 1% Agarose gel. The electrophoresis was carried out for 2 h at

50 V in Tris–acetate–EDTA buffer (pH 8.3). After electrophoresis, the gel was stained with Ethidium bromide (EB) for 30 min prior to being photographed under UV light [22,23]. The cleavage properties were determined based on the ability of compounds to convert the supercoiled form (Form I) into nicked form (Form II). The results were compared with standard DNA marker and control DNA.

3.3. Molecular docking studies

In the present anticancer docking study B-cell lymphoma-extra large (BCl–XL) protein (PDB ID: 3ZK6) was used as drug target in molecular docking studies to computationally prove the anticancer potentialities of newly synthesized metal complexes and ligands. The crystal structure of the BCL–XL protein bound to its respective inhibitor was collected from Protein Data Bank (PDB) database. The site to which the inhibitor molecule was bound was identified using PDBSum server. Optimization of target protein by removal ligands and hetero atoms was carried out using Discovery Studio tool. 3D coordinates files of newly synthesized compounds in ".pdb" format were generated using marvin sketch tool. Further, these files were converted from ".pdb" to ".pdbqt" file format using Autodock 4 tool. Automated molecular docking was carried out to determine the best orientation of the newly synthesized compounds possessing anti-cancer property was hypothesized as inhibitors bound in the active site of BCL-XL protein. A Lamarckian genetic algorithm implemented in the Auto Dock 4.0 program was employed [24]. The grid map was set by adjusting the grid box centered at the following active pocket residues of the BCL–XL protein [(Phe97(A), Arg102(A), Phe105(A), Ser106(A), Leu108(A), Glu129(A), Leu130(A), Asn136(A), Gly138(A), Arg139(A), Ala93(B), Phe97(B), Tyr101(B), Ala104(B), Phe105(B), Gly138(B) and Tyr195(B)]. These active pocket residues were used to generate with the AutoGrid file. The Lamarckian genetic algorithm was applied for minimization, using default parameters. The number of docking runs was 10, the population in the genetic algorithm was 250, the number of energy evaluations was 100,000, and the maximum number of interactions was 10,000 [25].

3.4. DPPH free radical-scavenging ability assay

In the present study, radical scavenging activity of ligands and their respective metal complexes was evaluated using the DPPH (1,1-diphenyl-2-picrylhydrazyl) radical as a reagent [26]. Required volume of a DPPH radical solution in ethanol (60 μM) was mixed with different concentrations of testing samples. The mixture was incubated for 30 min in dark at room temperature. After the incubation, the absorbance of the reaction mixture was measured at 517 nm using a UV–Vis Spectrophotometer. For the positive control ascorbic acid was used as a reference standard. The DPPH scavenging activity of each sample was calculated using the following equation:

$$\% \text{ inhibition} = [(A_c - A_t)/A_c] \times 100$$

Where, A_c is the absorbance of the control reaction (100 μL of ethanol with 100 μL of the DPPH solution) and A_t is the absorbance of the test sample. The experiment was done in triplicate. The IC_{50} value was calculated for all the samples. Lower absorbance of the reaction mixture indicates higher free radical activity.

4. Results and discussion

4.1. Spectral characterization

4.1.1. IR spectral studies

To identify the bonding mode as well as the complexation behavior, the IR spectra were recorded for the synthesized hydrazone Schiff base ligands and their respective metal complexes. The IR spectrum of ligand 1 (L^1H) is reproduced in spectrum 1 of supplementary material. The sharp intense band at 1701 cm^{-1} is assigned to ν(C=O) of carboxylic acid group. One more band at 1668 cm^{-1} is due to hydrazone ν(C=N) group. The weak broad bands at 3407 cm^{-1} and 2434 cm^{-1} are due to ν(N–H) and ν(O–H) respectively.

Similar observations are made for ligand 2 (L^2H, spectrum 2 of supplementary material) as well, the spectrum shows weak broad

Table 3
Elemental analyses of ligands (L^1H and L^2H) and their respective metal complexes along with molar conductance data.

Compound	Empirical formula	M%		C%		H%		N%		Color/% yield	Molar conductance, Λ_m ($\Omega^{-1}cm^2mol^{-1}$)
		Found	Calcd.	Found	Calcd.	Found	Calcd.	Found	Calcd.		
L^1H	$C_{22}H_{16}N_2O_4$	–	–	70.94	70.96	4.31	4.33	7.46	7.52	Canary yellow/94	–
$Cu(L^1)_2$	$C_{44}H_{30}CuN_4O_8$	7.93	7.88	65.51	65.54	3.78	3.75	6.89	6.95	Green/48	20.1
$Ni(L^1)_2$	$C_{44}H_{30}NiN_4O_8$	7.38	7.32	65.90	65.94	3.71	3.77	6.93	6.99	Golden yellow/50	15.7
$Co(L^1)_2$	$C_{44}H_{30}CoN_4O_8$	7.41	7.35	65.87	65.92	3.80	3.77	6.92	6.99	Yellow/54	18.8
L^2H	$C_{25}H_{22}N_2O_3$	–	–	75.31	75.36	5.51	5.57	6.96	7.03	Canary yellow/92	–
$Cu(L^2)_2$	$C_{50}H_{42}CuN_4O_6$	7.47	7.40	69.90	69.96	4.87	4.93	6.46	6.53	Apple green/51	19.8
$Ni(L^2)_2$	$C_{50}H_{42}NiN_4O_6$	6.93	6.88	70.28	70.35	4.92	4.96	6.48	6.56	Primrose yellow/48	16.1
$Co(L^2)_2$	$C_{50}H_{42}CoN_4O_6$	6.99	6.90	70.25	70.33	4.90	4.96	6.47	6.56	Tangerine/45	19.6

Table 4
Determination of molar conductance (Λ_m) of metal complexes.

Complexes	Conductance (G) in Ω^{-1} at 25 °C	Conductivity (κ) in $\Omega^{-1}cm^{-1}$	Molar conductance (Λ_m) in $\Omega^{-1}cm^2mol^{-1}$
		$\kappa = G$ ($\because$ G* = 1.0)	$\Lambda_m = (1000\ \kappa)/c$
$Cu(L^1)_2$	18.2×10^{-6}	18.2×10^{-6}	18.2
$Ni(L^1)_2$	16.8×10^{-6}	16.8×10^{-6}	16.8
$Co(L^1)_2$	14.9×10^{-6}	14.9×10^{-6}	14.9
$Cu(L^2)_2$	16.1×10^{-6}	16.1×10^{-6}	16.1
$Ni(L^2)_2$	18.5×10^{-6}	18.5×10^{-6}	18.5
$Co(L^2)_2$	21.9×10^{-6}	21.9×10^{-6}	21.9

Cell constant (G*) of *ELICO CM 180* conductivity meter = 1.0.
Conductance (G) values are obtained from the experiment in $\mu\Omega^{-1}$ or μS.
Conductance (G) of 1 mM solutions (in DMF) of metal complexes is recorded.

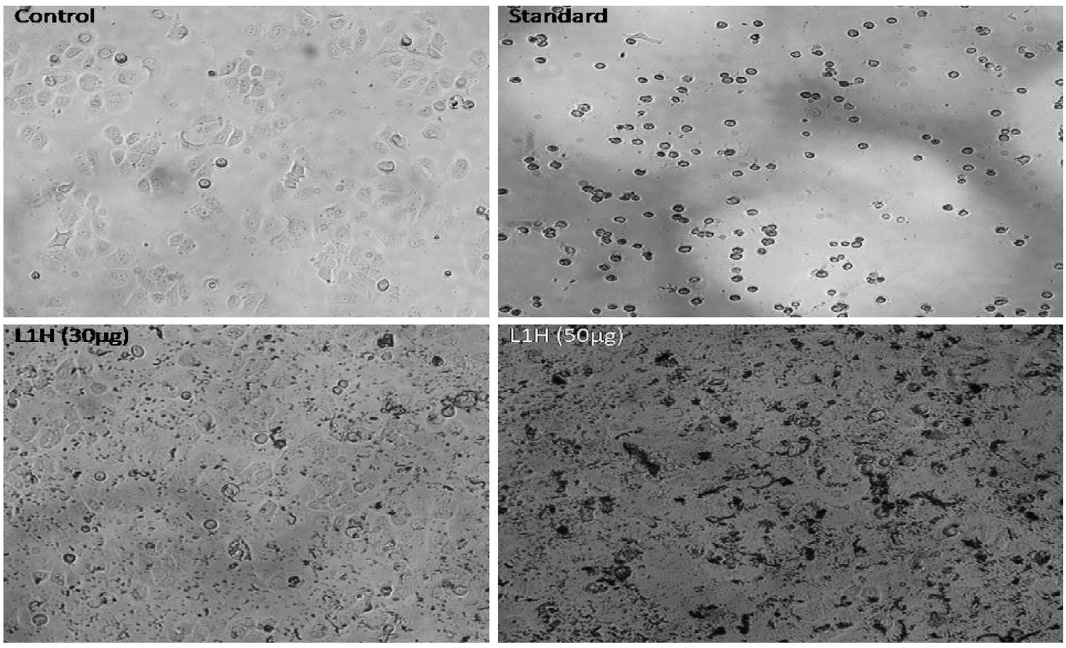

Fig. 1. Anticancer activity images of treated cells (MCF−7) with different concentrations of L^1H, control cells and positive control.

band at 2523 cm^{-1} due to carboxylic acid ν(O−H) vibrations. The ν(N−H) vibrations appeared at 3325 cm^{-1}. The sharp intense band at 1705 cm^{-1} is assigned to ν(C═O) of carboxylic acid group. The sharp band at 1680 cm^{-1} is due to hydrazone ν(C═N) group. In both the ligands the amide stretching is not clearly visible, which could be due to overlapping with the carboxylic acid group. The diagnostic IR frequencies of ligands and their respective metal complexes are compiled in Table 1.

In all the metal complexes, the hydrazone ν(C═N) band is shifted to lower wave number by 20−30 cm^{-1}, which infers the involvement of nitrogen atom of hydrazone group in coordination to the central metal ion [27]. The absence of broad band in the region 2400−3400 cm^{-1} infers the coordination of carboxylic acid oxygen *via* deprotonation. Further, the strong band due to ν(C═O) of carboxylic acid group has disappeared upon complex formation, since in carboxylate ion the negative charge is equally distributed on two oxygen atoms due to resonance, thereby decreasing the bond order. This implies that, the carboxylate ion is involved in bond formation [28]. Simultaneously, two new bands have appeared in the range of 1520−1580 cm^{-1} and 1370−1380 cm^{-1} which are assigned to the asymmetric and symmetric stretching frequencies of coordinated carboxylate ion respectively. In $Cu(L^1)_2$ and $Cu(L^2)_2$ complexes (Spectrum 3 and 4 respectively of supplementary material) new sharp band appearing at 1610 and 1645 cm^{-1} respectively corresponds to the vibrations of amide carbonyl stretching ν(C═O), which have shifted to lower wavenumber when compared with that in ligand spectrum. This infers the coordination of amide carbonyl oxygen to the central metal ion. The medium vibrations due to ν(M − O) are observed between 500 and 550 cm^{-1} [29,30]. Similar observations are made in case of

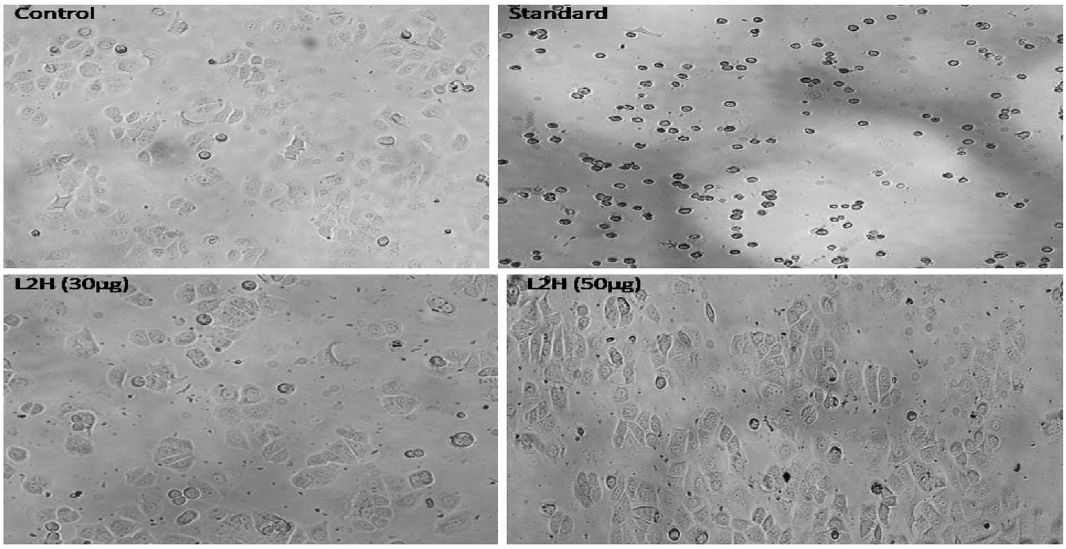

Fig. 2. Anticancer activity images of treated cells (MCF−7) with different concentrations of L^2H, control cells and positive control.

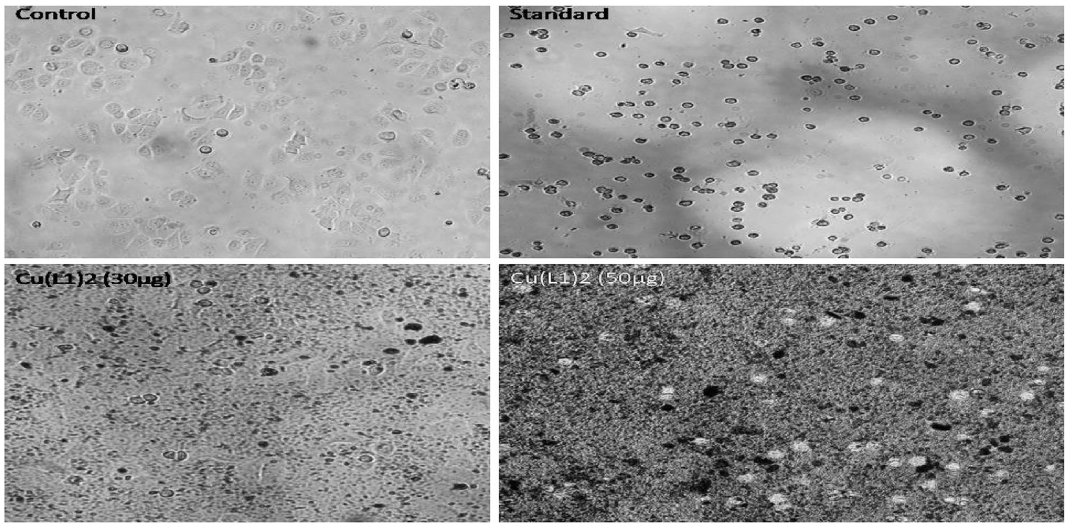

Fig. 3. Anticancer activity images of treated cells (MCF–7) with different concentrations of $Cu(L^1)_2$, control cells and positive control.

nickel (II) and cobalt (II) complexes as well. IR data suggests the ONO donor tridentate behavior of the ligands.

4.1.2. ^1H and ^{13}C NMR spectral studies

The ^1H NMR spectrum of ligand 1 (L^1H, spectrum 5 of supplementary material) shows a broad singlet centered at 12.15 ppm due to amido proton (−NH−). Proton attached to carboxylic acid oxygen sometimes due to exchange with moisture in the solvent will not appear. The characteristic singlet at 3.87 ppm is due to the resonance of methoxy protons. Remaining protons are aromatic and appeared as multiplets between 7.0 and 9.0 ppm [31]. ^1H NMR (400 MHz, DMSO-d_6) δ/ppm: 3.87 (s, 3H, −OMe), 7.14 (d, 2H, J = 8.6 Hz), 7.54 (t, 1H, J = 7.3 Hz), 7.64(td, 2H, J = 7.3, 4.7 Hz), 7.93−8.25 (m, 6H), 12.15 (br, 1H, −NH). ^{13}C NMR spectrum of ligand 1 (L^1H, spectrum 7 of supplementary material) shows a characteristic peak due to methoxy carbon at 56 ppm. The bridging carbon of fluorene ring resonated at 155 ppm. The peak at 164 ppm is due to the resonance of amide carbon. Carboxylic acid carbon resonates at 168 ppm. The carbon attached to methoxy oxygen appeared at 163 ppm due to deshielding effect of oxygen atom. Remaining carbon nuclei are part of the aromatic ring and are resonating between 110 and 150 ppm [32].

The ^1H NMR spectrum of ligand 2 (L^2H, spectrum 6 of supplementary material) shows a characteristic sharp singlet at 1.34 ppm due to the protons attached to *t*-butyl group. The broad singlet at 12.21 ppm is due to the proton attached to amido nitrogen (−NH−). The carboxylic acid proton due to moisture present in the solvent will be exchanged and may not appear in most of the cases. Remaining protons are aromatic and appeared as multiplets between 7.0 and 9.0 ppm [31]. ^1H NMR (400 MHz, DMSO-d_6) δ/ppm: 1.30 (s, 9H, *t*-Bu), 7.55 (t, 1H, J = 7.6 Hz), 7.60−7.65 (m, 4H), 7.99 (q, 2H, J = 3.7 Hz), 8.05 (d, 2H, J = 7.9 Hz), 8.12 (d, 1H, J = 6.7 Hz), 8.38 (s, 1H), 12.21 (br, 1H, −NH). ^{13}C NMR spectrum of ligand 2 (L^2H, spectrum 8 of supplementary material) depicts two characteristic

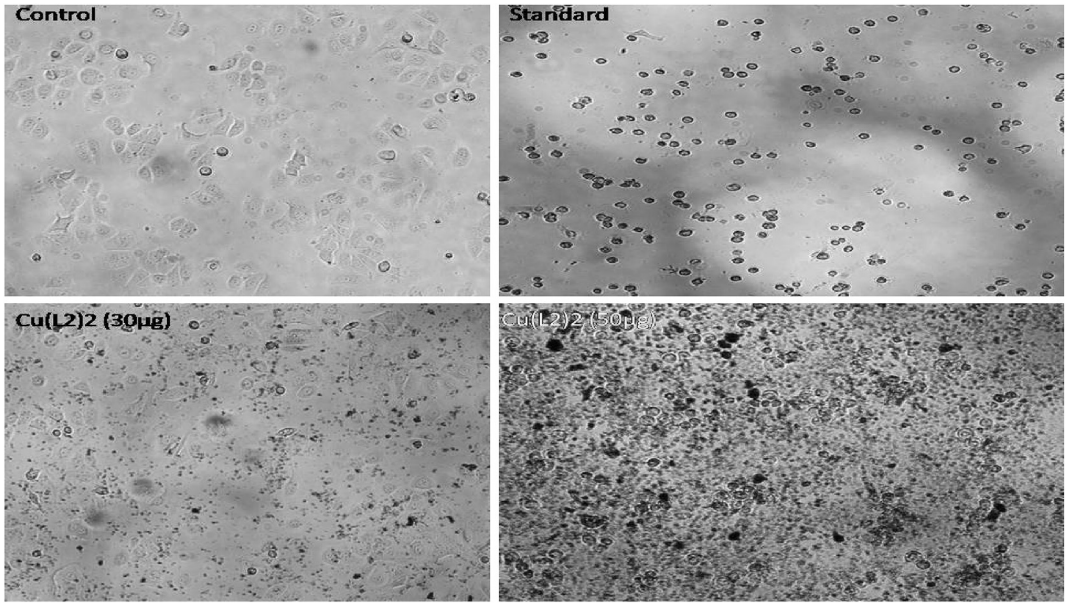

Fig. 4. Anticancer activity images of treated cells (MCF–7) with different concentrations of $Cu(L^2)_2$, control cells and positive control.

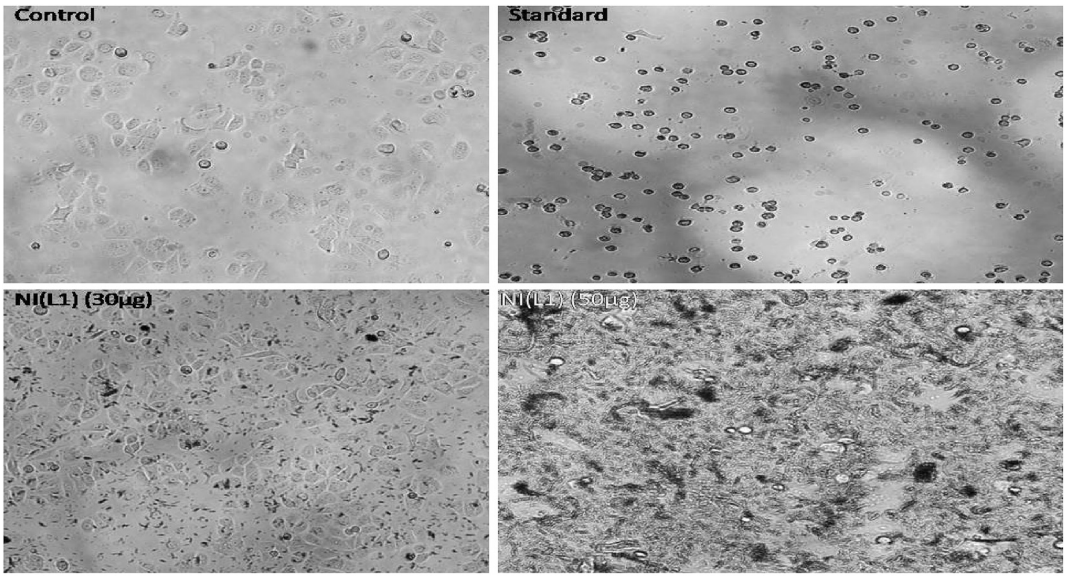

Fig. 5. Anticancer activity images of treated cells (MCF−7) with different concentrations of $Ni(L^1)_2$, control cells and positive control.

peaks; one at 31 ppm and another at 35 ppm are methyl carbon and *t*-butyl carbon resonances respectively. The bridging carbon of fluorene ring is resonating at 156 ppm. The peak at 163 ppm is due to the presence of amide carbon. The carboxylic acid carbon resonated at 167 ppm. Remaining carbon nuclei are part of the aromatic ring and are resonating between 120 and 150 ppm [32].

4.1.3. Mass spectral studies

Electrospray ionization (ESI) mass spectral data of ligands 1 (L^1H) and 2 (L^2H) and their respective copper (II) complexes [$Cu(L^1)_2$ and $Cu(L^2)_2$] are reproduced respectively in spectrum 9 to 12 of supplementary material. Ligand 1 (L^1H) shows $[M+2]^+$ peak at *m*/*z* 374. Similarly, L^2H shows $[M+1]^+$ peak at *m*/*z* 399. Electrospray ionization mass spectral (ESI-MS) study of metal complexes supports 1 : 2 $[(ML)_2]$ stoichiometry. $Cu(L^1)_2$ complex show $[M-2]^+$ peak at *m*/*z* 803; whereas $Cu(L^2)_2$ complex show $[M-1]^+$ peak at *m*/*z* 856. Similar observations are made for nickel (II) and cobalt (II) complexes as well. The mass spectral data is matching very well with the predicted molecular weights of the compounds and this confirms the formation of metal complexes in each case [33,34]. The mass spectra of nickel (II) and cobalt (II) complexes are reproduced in spectrum 13 to 16 of supplementary material.

4.1.4. Electronic spectral studies

Electronic spectra of ligands 1 (L^1H) and 2 (L^2H) (spectrum 17 of supplementary material) and their respective metal complexes were recorded in methanol. The d-d transitions are recorded in concentrated solutions of metal complexes prepared in DMF. The

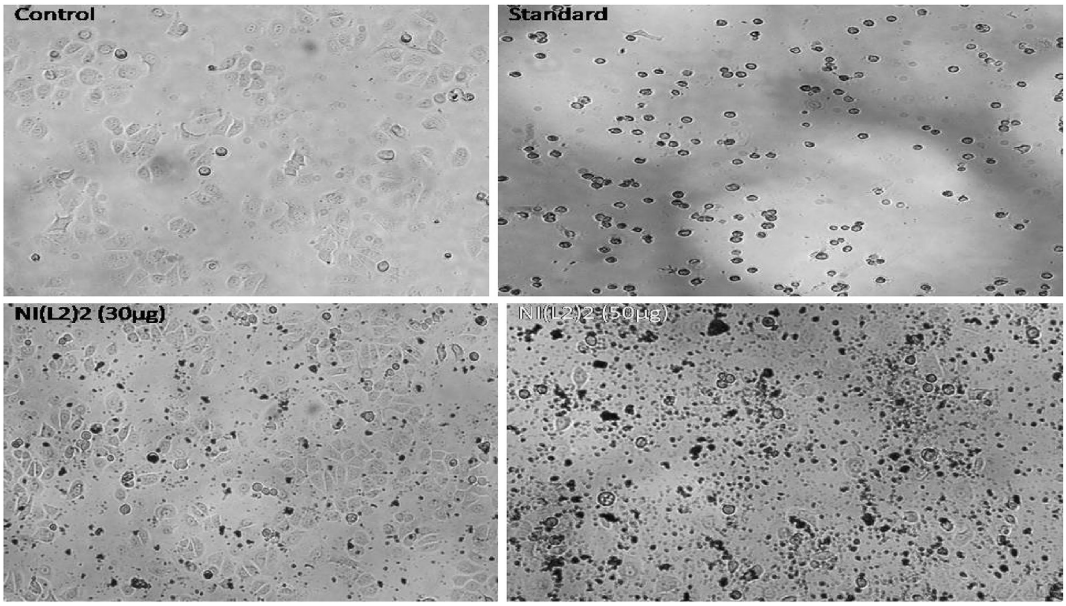

Fig. 6. Anticancer activity images of treated cells (MCF−7) with different concentrations of $Ni(L^2)_2$, control cells and positive control.

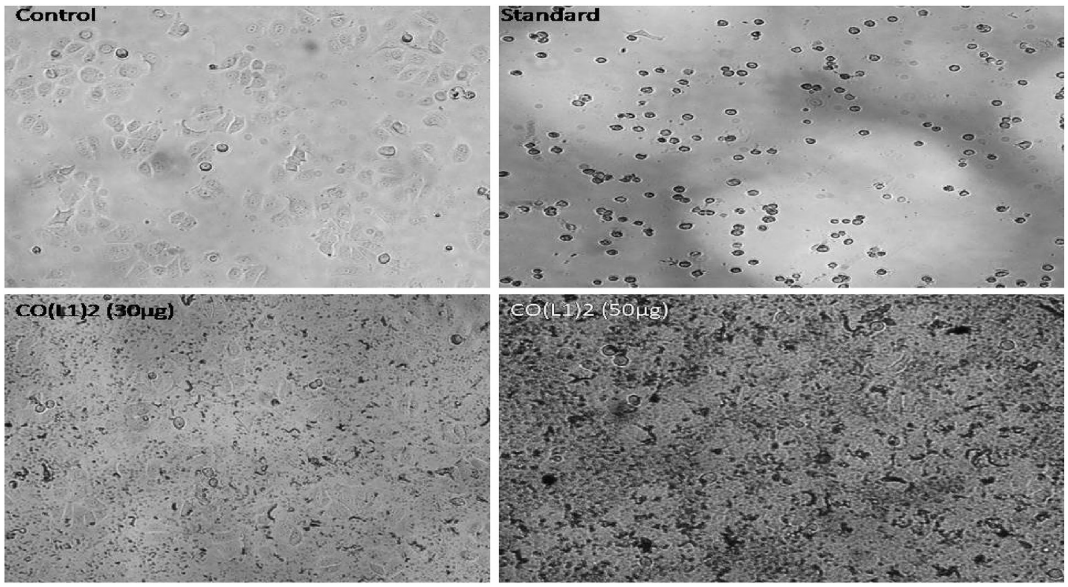

Fig. 7. Anticancer activity images of treated cells (MCF–7) with different concentrations of $Co(L^1)_2$, control cells and positive control.

free ligands absorb strongly at 350 and 348 nm (in L^1H and L^2H respectively) due to $\pi \rightarrow \pi^*$ transitions. These bands have remained almost unchanged upon complexation. The bands at 415 nm (in L^1H) and 410 nm (in L^2H) are ascribed to $n \rightarrow \pi^*$ transitions associated with carbonyl groups and hydrazone (C═N) group. These bands have suffered bathochromic (red) shift in all the cases upon complex formation due to the donation of charge density to the metal ion for the coordination. This confirms that, the nitrogen atom of hydrazone group, the oxygen atoms of amide and carboxylic acid group are involved in the bond formation. IR spectra of the metal complexes support the observations made from electronic spectral studies. Intra-molecular charge transfer bands are seen at 440 nm (in L^1H) and 436 nm (in L^2H) [35]. These bands have shifted to lower wavelengths (hypsochromic shift) upon complexation, indicating that charge density is transferred from metal to ligand.

The absorption spectrum of $Cu(L^1)_2$ and $Cu(L^2)_2$ complexes (spectrum 18 and 19 respectively, of supplementary material) shows one broad peak due to spin-allowed d–d transition centered at 707 and 717 nm assignable to $^2T_{2g}\tilde{o} \leftarrow {}^2E_g$ as is the consequence of distorted octahedral environment around copper (II) ion [36,37].

Table 2 shows the solution electronic absorption spectral data of ligands and their respective metal complexes. In case of nickel (II) and cobalt (II) complexes d–d transitions are rarely recorded or too small to be observed, since these transitions are Laporte forbidden.

4.1.5. Thermal analysis studies

Thermal behavior of all the metal complexes was studied over a

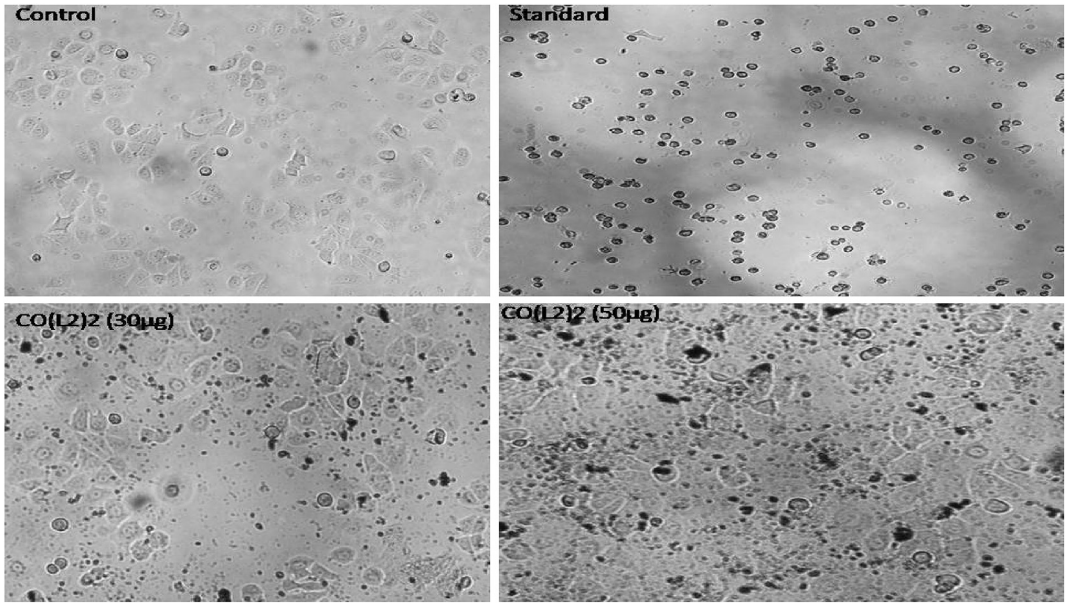

Fig. 8. Anticancer activity images of treated cells (MCF–7) with different concentrations of $Co(L^2)_2$, control cells and positive control.

Table 5
Cell viability data of ligand L^1H and its metal complexes for MCF−7 cell line at five different concentrations.

MCF−7				
Concentration in μgmL^{-1}	L^1H	$Co(L^1)_2$	$Cu(L^1)_2$	$Ni(L^1)_2$
10	49.1128 ± 7.9489	64.7977 ± 3.4776	35.9120 ± 0.8517	52.8034 ± 1.4194
20	45.5642 ± 3.1228	61.2491 ± 4.4712	7.5231 ± 1.1356	31.5117 ± 3.1228
30	42.3705 ± 1.9162	60.1845 ± 0.8517	1.5614 ± 1.4194	29.4535 ± 7.4521
40	41.3769 ± 2.6260	48.5451 ± 2.6969	0.4968 ± 1.0646	25.2662 ± 2.8389
50	36.5508 ± 1.6324	43.2931 ± 4.1164	0.0710 ± 0.0710	23.066 ± 4.4712
Untreated	100 ± 0.4968	100 ± 0.4968	100 ± 0.4968	100 ± 0.4968
Cisplatin 15μgmL^{-1}	13.5558 ± 1.3485	13.5558 ± 1.3485	13.5558 ± 1.3485	13.5558 ± 1.3485

Table 6
Cell viability data of ligand L^2H and its metal complexes for MCF−7 cell line at five different concentrations.

MCF−7				
Concentration in μgmL^{-1}	L^2H	$Co(L^2)_2$	$Cu(L^2)_2$	$Ni(L^2)_2$
10	85.1668 ± 7.0972	55.1455 ± 4.4712	32.8602 ± 1.3485	39.8864 ± 2.9808
20	73.1725 ± 2.0582	53.8680 ± 5.7488	29.7374 ± 4.1874	39.7445 ± 0.2839
30	69.4819 ± 8.1618	52.9454 ± 1.8453	2.4840 ± 0.3549	32.7892 ± 0.4258
40	64.8687 ± 9.6522	46.9837 ± 4.8261	1.1356 ± 0.0	24.1306 ± 2.2711
50	58.6231 ± 1.2775	34.2796 ± 0.3549	1.2775 ± 1.9872	22.4982 ± 1.9162
Untreated	100 ± 0.4968	100 ± 0.4968	100 ± 0.4968	100 ± 0.4968
Cisplatin 15μgmL^{-1}	13.5558 ± 1.3485	13.5558 ± 1.3485	13.5558 ± 1.3485	13.5558 ± 1.3485

Table 7
IC_{50} values of ligands and their respective metal complexes in μgmL^{-1} for MCF−7 cell line.

Compound	IC_{50} (μgmL^{-1})
L^1H	<10
$Co(L^1)_2$	40.07
$Cu(L^1)_2$	<10
$Ni(L^1)_2$	<10
L^2H	63.0
$Co(L^2)_2$	27.20
$Cu(L^2)_2$	<10
$Ni(L^2)_2$	<10

temperature range of 25−1000 °C under nitrogen atmosphere. Thermograms of Cu(II), Ni(II) and Co(II) complexes of L^1H are reproduced in entry 20 of supplementary material. The copper (II) complex is highly stable up to 290 °C. Later on, from 300 to 480 °C, the metal complex decomposes in only one significant step and 91% of weight loss is observed. It matches very well with the theoretical value of 92.1% for the loss of two ligand groups and it clearly infers that, only ligand moiety is present in the complex has lost. After 500 °C, the plateau is observed till the stable metal oxide formation takes place [38]. This result is in line with the IR, electronic spectral and GC−MS data. Similar plot is observed for Ni(II) and Co(II) complexes as well and the observed results are in line with the calculated weight losses. Thus, the thermal data of the metal complexes give no evidence for the presence of any other coordinated moieties like water, chloride etc.

4.1.6. Molar conductance studies

Molar conductance of all the metal complexes was measured at 25 °C by preparing mmol solutions in DMF using the conductivity bridge (G* = 1). The values obtained for the metal complexes not exceeded 20 Ω^{-1} cm^2 mol^{-1} which confirms the non-electrolytic nature of metal complexes [39]. The molar conductance values have been reproduced in Table 3 along with the elemental analyses data which are in well agreement with the calculated percentages of each element. The detailed experimental results of molar conductance study have been tabulated in Table 4.

4.2. Bioassay results

4.2.1. Anticancer activity of ligands and their metal complexes against breast cancer cells (MCF-7)

In the present investigation, *in vitro* MTT cell viability model was taken to study the cytotoxic effect of ligands and their metal complexes on the breast cancer (MCF−7) cell line. Different concentrations (10, 20, 30, 40 and 50 μgmL^{-1}) of ligands and their metal complexes were employed to treat MCF-7 cells, whereas untreated MCF−7 cells were considered as control group and cisplatin treated MCF-7 cells were considered as positive control. The cell images of anticancer activity when treated with ligands and their respective metal complexes are reproduced in Figs. 1–8.

Percentage cell viability of ligands and their respective metal complexes v/s concentration are plotted in bar plots 1 and 2, compared with that of standard chemotherapeutic drug cisplatin. Experimental values are reproduced in Tables 5 and 6 respectively. Concentration dependent cell viability was observed in all treated samples, the cell viability decreased with increase in concentration.

In case of all tested drugs, dose dependant activity was observed with salient features. The IC_{50} value of L^1H, $Cu(L^1)_2$, $Cu(L^2)_2$, $Ni(L^1)_2$ and $Ni(L^2)_2$ compounds is found to be less than 10μgmL^{-1} and other tested drugs also demonstrated very promising activity (Table 7). Compared with control group, the cells treated with ligands and metal complexes showed significant detach in culture medium. There was a decrease in number of cells as well as observable abnormalities in the treated group of cells such as turgidity, shrunken in shape, cell breakage, cell shrinkage and apoptotic bodies are observed compared to untreated control cells. Microscopic examination revealed that, morphological changes and shrinkage of cells occurred, leading to cell apoptosis induced by tested compounds [40,41]. IC_{50} values of ligands and their respective metal complexes in μgmL^{-1} for the MCF−7 cell line are compiled in Table 5.

4.2.2. DNA cleavage studies

Designing small molecules help in targeting specific sites on a DNA strand and can lead to novel therapeutic agents. Photocleavage study of DNA also helps in various applications like photodynamic therapy of cancers, DNA foot printing agents and in genomic

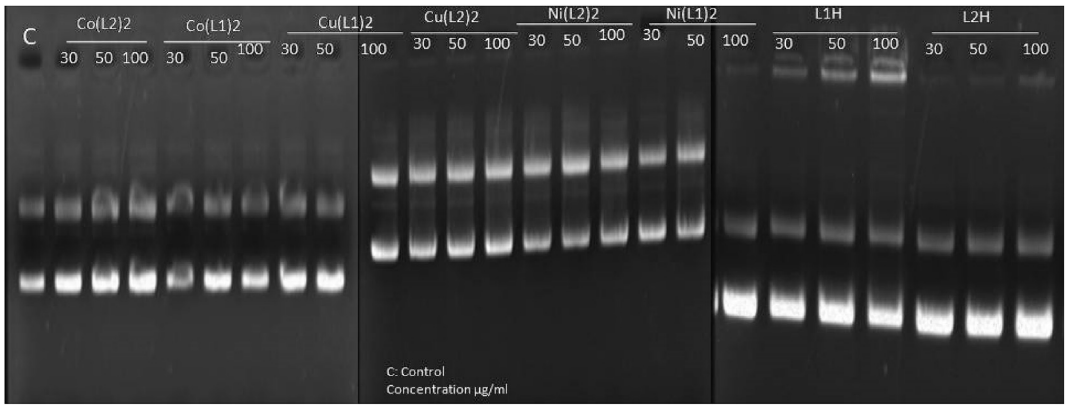

Fig. 9. Gel electrophoresis images of ligands 1 and 2 (L^1H and L^2H) and their respective metal complexes showing the effect on pBR322 DNA compared with negative control.

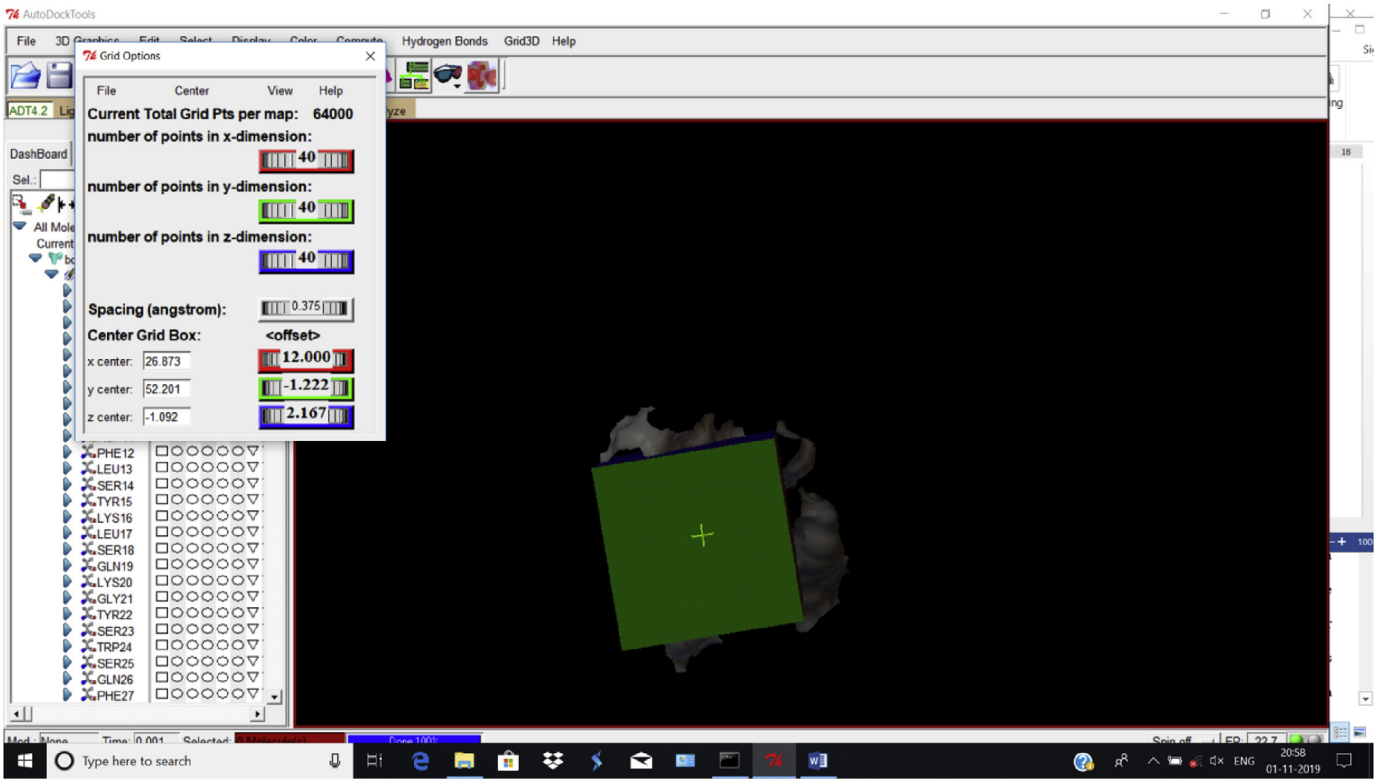

Fig. 10. Grid setting.

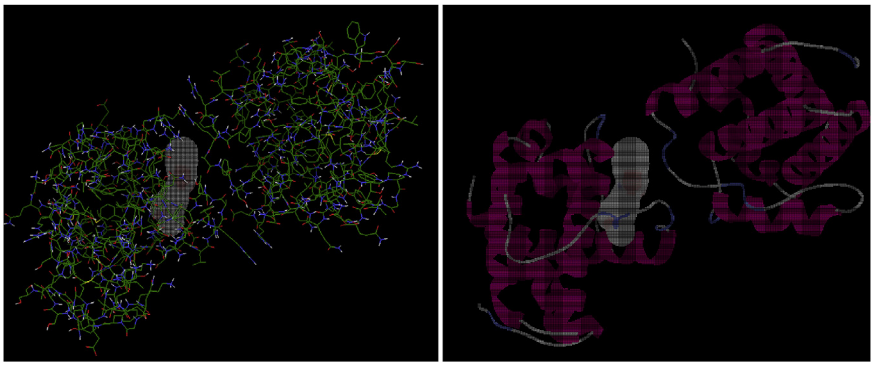

Fig. 11. Docked view of L^1H at the active site of the enzyme BCL−XL.

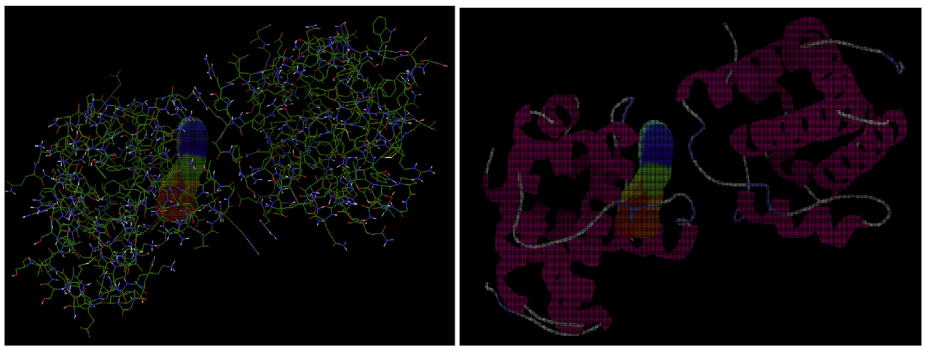

Fig. 12. Docked view of L^2H at the active site of the enzyme BCL–XL.

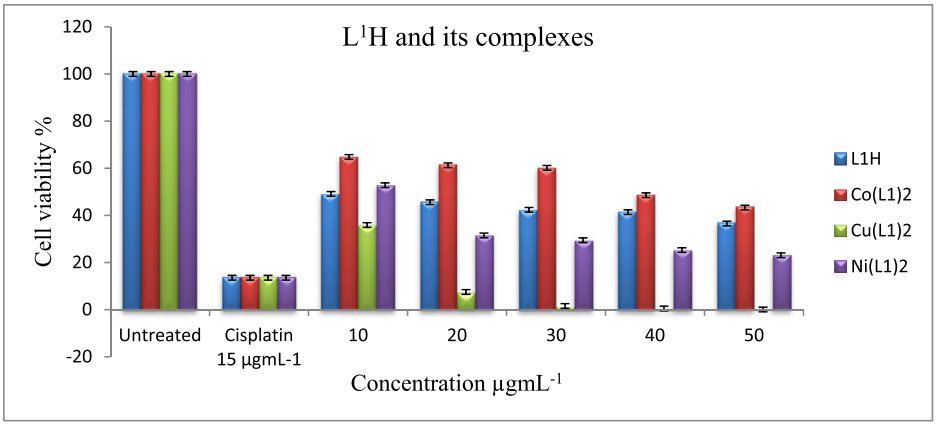

Plot 1. Bar graph showing the % cell viability of ligand L^1H and its metal complexes for MCF–7 cell line v/s concentration in μgmL^{-1}.

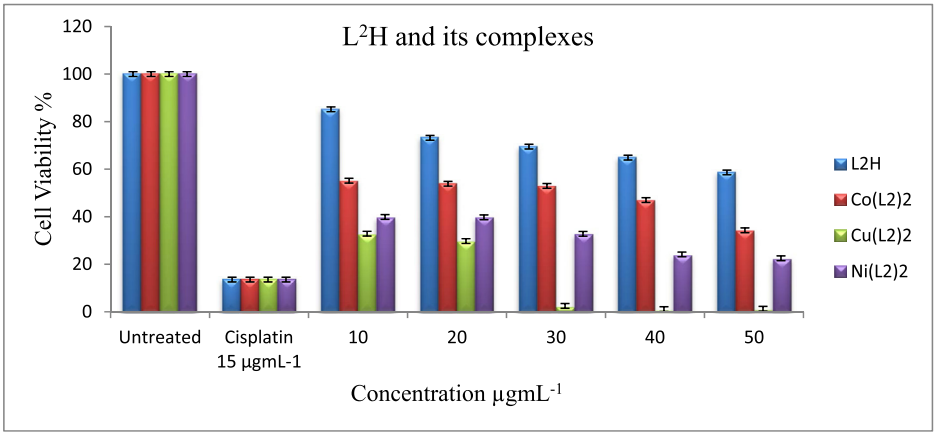

Plot 2. Bar graph showing the % cell viability of ligand L^2H and its metal complexes for MCF–7 cell line v/s concentration in μgmL^{-1}.

Table 8
Docking score of ligands.

Sl. No.	Molecule	Orientation	Binding energy	Docking energy	Inhibition constant	Intermol energy	Desolv energy	Electrostatic energy	Total internal energy	Torsional energy	RMS	Hydrogen bond
1	**L^1H**	1	−9.38	−0.34	132.69	−10.87	−11.3	0.43	−0.29	1.49	0.0	–
2	**L^2H**	1	−10.84	−0.36	11.4	−12.33	−12.8	0.47	−0.28	1.49	0.0	–

research [42,43]. Interaction of metal complexes with pBR322 DNA was studied using Agarose gel electrophoresis technique. In the present study untreated DNA taken as control group where as test group was taken for the metal complexes treated DNA. Different concentrations of metal complex were treated on the pBR322 DNA. In all metal complex treated DNA shown change in the band pattern

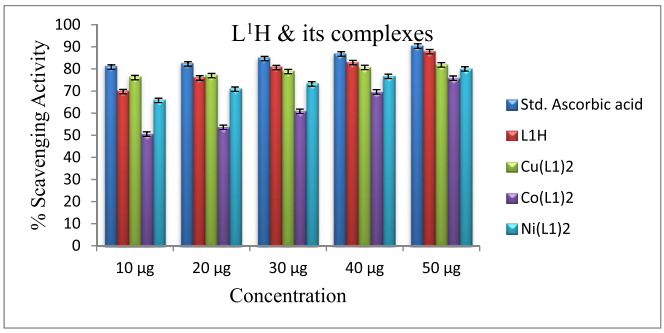

Plot 3. Graphical representation of dose dependent DPPH radical scavenging model by L^1H and its metal complexes.

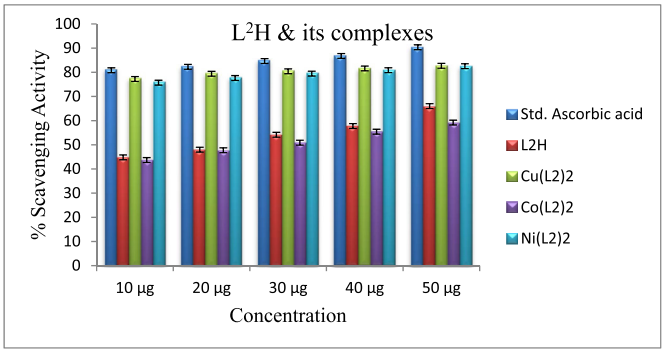

Plot 4. Graphical representation of dose dependent DPPH radical scavenging model by L^2H and its metal complexes.

by changing closed DNA (Form−I) to Nicked circular DNA (Form−II) and linear form (Form−III). In general fast migration of DNA occurs in control DNA and in case of treated groups due to the DNA cleavage slow migration is observed. Due to the action of metal complexes super coiled DNA form undergo relaxation to produce nicked and linear form with breaks and smear appearance [44,45]. Overall findings have revealed that, the tested compounds can successfully cleave the DNA as it is evident from the images reproduced in Fig. 9.

4.2.3. Molecular docking studies

In case of cancer, some class of proteins makes the failure of apoptosis by inhibiting the action of drugs on targeted molecules those are collectively known as survival proteins or anti-apoptotic proteins (BCL−2−family proteins). In humans, six anti-apoptotic members of the BCL−2 family have been reported, including BCL−2, BCL−XL, MCL−1, BCL−W, BFL−1 and BCL−B [46].

Hence, in the present study, BCL−XL was taken as receptor molecule for docking to study the anticancer potential of newly synthesized ligands and their metal complexes. In the present study, active sites of several amino acids were included in the docking study. The selected metal complexes and ligands have shown appreciating anticancer activity through docking within active sites of BCL−XL consisting of Phe97(A), Arg102(A), Phe105(A), Ser106(A), Leu108(A), Glu129(A), Leu130(A), Asn136(A), Gly138(A), Arg139(A), Ala93(B), Phe97(B), Tyr101(B), Ala104(B), Phe105(B), Gly138(B) and Tyr195(B) amino acid residues. The selected compounds were successfully docked and studied for type of interactions with receptor protein like electrostatic interactions, binding energy and other parameters. Furthermore, molecular docking studies have shown that, selected complexes were having strong binding affinity with BCL−XL and also acting as strong BCL−XL inhibitor. The obtained docking result showed a good correlation between *in vitro* anticancer activity and binding free energy of selected compounds. Grid setting is shown in Fig. 10 whereas, the docked view of ligands L^1H and L^2H with BCL−XL protein is shown in Figs. 11 and 12 respectively. Docking score of the ligands L^1H and L^2H are reproduced in Table 8.

4.2.4. DPPH free radical-scavenging ability

Free radicals lead to the severe causes and implications in the occurrence of various diseases such as liver cirrhosis, atherosclerosis, cancer, diabetes and aging [47]. Antioxidants play an important role in the control of free radicals by delaying or inhibiting its activity. Many previous reports show that, Schiff bases are the selective molecules which can prevent the activity of free radicals and act as potent antioxidants.

In the present study, percent inhibition values of DPPH of synthesized compounds were analyzed and compared with Vitamin C (Ascorbic acid) used as standard in different concentrations. The study shows that, the compounds L^1H, $Ni(L^1)_2$, $Ni(L^2)_2$, $Cu(L^1)_2$ and $Cu(L^2)_2$ exhibited significant scavenging activity with good percentage when compared with remaining tested compounds, whereas, standard ascorbic acid shown highest antioxidant activity with percentage 90.36 ± 0.3777. The present results clearly show that, there was dose dependant activity in all tested compounds i.e. the inhibition values were increased with increasing concentrations of all compounds. Plots 3 and 4 represent the % scavenging activity of synthesized compounds at different concentrations. The

Table 9
Experimental results of L^1H and its metal complexes on DPPH radical scavenging model.

Sl. No	Conc.	Std. Ascorbic acid	L^1H	$Cu(L^1)_2$	$Co(L^1)_2$	$Ni(L^1)_2$
1	10 µg	80.8333 ± 0.1777	69.7333 ± 0.2222	76.0666 ± 0.2222	50.5230 ± 0.2444	65.7667 ± 0.5535
2	20 µg	82.2667 ± 0.2222	75.9333 ± 0.2222	76.9666 ± 0.2444	53.6000 ± 0.2666	70.8333 ± 0.2444
3	30 µg	84.6667 ± 0.3111	80.6333 ± 0.1111	78.8000 ± 0.2000	60.8333 ± 0.2444	73.2000 ± 0.1333
4	40 µg	86.7666 ± 0.1111	82.8667 ± 0.1333	80.6667 ± 0.1111	69.6000 ± 0.2666	76.6667 ± 0.4444
5	50 µg	90.3666 ± 0. 3777	87.8000 ± 0.2000	81.8333 ± 0.1111	75.8000 ± 0.1333	80.0000 ± 0.1333

Table 10
Experimental results of L^2H and its metal complexes on DPPH radical scavenging model.

Sl. No	Conc.	Std. Ascorbic acid	L^2H	$Cu(L^2)_2$	$Co(L^2)_2$	$Ni(L^2)_2$
1	10 µg	80.8333 ± 0.1777	44.8000 ± 0.4000	77.2333 ± 0.2444	43.7000 ± 0.2000	75.7166 ± 0.1888
2	20 µg	82.2667 ± 0.2222	48.0000 ± 0.1333	79.4000 ± 0.1333	47.7333 ± 0.2222	77.6333 ± 0.1777
3	30 µg	84.6667 ± 0.3111	54.1667 ± 0.3111	80.4000 ± 0.1333	50.9000 ± 0.4666	79.4666 ± 0.2222
4	40 µg	86.7666 ± 0.1111	57.7770 ± 0.3333	81.6000 ± 0.1333	55.4333 ± 0.2444	80.8666 ± 0.7555
5	50 µg	90.3666 ± 0. 3777	66.0000 ± 0.1333	82.7000 ± 0.2000	59.2000 ± 0.4000	82.5333 ± 0.2222

experimental results of DPPH radical scavenging model was tabulated in Tables 9 and 10.

5. Conclusions

In the current study, two new methoxy and *t*-butyl substituted hydrazone Schiff base ligands and their metal complexes were synthesized. The key precursors, ligands and their transition metal complexes were characterized by spectral (^{1}H and ^{13}C NMR, IR, ESI–MS), analytical, TGA and molar conductance measurements. The transition metal complexes were screened for their pharmacological activities *viz*., DNA cleavage, cytotoxicity, anticancer and antioxidant activities. The hydrazone Schiff bases and their metal complexes successfully cleaved the pBR322 plasmid DNA. Concentration dependent cell survival rate was observed in *in vitro* cytotoxicity against breast cancer (MCF–7) cell line, which was decreased with increase in concentration. Anticancer study revealed that, the synthesized compounds show apoptotic effect which was characterized by cell shrinkage, cell breakage, turgidity and apoptotic bodies. IC_{50} value (<10 μgmL^{-1}) for the compounds L^1H, $Cu(L^1)_2$, $Cu(L^2)_2$, $Ni(L^1)_2$ and $Ni(L^2)_2$ suggests very significant activity, when compared to standard cisplatin. The antioxidant activity study shows dose dependant activity in all tested compounds i.e. the inhibition values were increased with increasing concentrations of all compounds. The compounds L^1H, $Ni(L^1)_2$, $Ni(L^2)_2$, $Cu(L^1)_2$ and $Cu(L^2)_2$ exhibited significant scavenging activity with good percentage when compared with remaining tested compounds. Molecular docking studies have shown that, selected compounds were having strong binding affinity with BCL–XL and also acting as strong BCL–XL inhibitor. The obtained docking result showed a good correlation between *in vitro* anticancer activity and binding free energy of selected compounds.

Declaration of competing interest

Authors do not have any conflicts of interest to declare.

Acknowledgements

The author acknowledges University Grants Commission, New Delhi, India, for providing the financial support through *BSR-RFSMS* fellowship [F. NO: 25–1/2014–15(BSR)/7–100/2007/(BSR) Dated: November 05, 2015]. Authors are grateful to the Chairman, Department of Chemistry, Karnatak University Dharwad, for providing the laboratory facilities. Authors are thankful to University Scientific Instrumentation Centre and SAIF, K. U. D, for providing instrumental facilities.

Appendix A. Supplementary data

Supplementary data to this article can be found online at https://doi.org/10.1016/j.jorganchem.2020.121219.

References

[1] https://www.labiotech.eu/features/cancer-treatments-immuno-oncology/ accessed on 01st October 2019.
[2] J.H. Atkins, L.J. Gershell, Nat. Rev. Drug Discov. 1 (2002) 491–492, https://doi.org/10.1038/nrd842.
[3] Jungang Deng, Ping Yu, Zhenlei Zhang, Jun Wang, Jinhua Cai, Na Wu, Hongbin Sun, Hong Liang, Feng Yang, Eur. J. Med. Chem. 158 (2018) 442–452, https://doi.org/10.1016/j.ejmech.2018.09.020.
[4] C. Sheridan, G. Brumatti, M. Elgendy, M. Brunet, S.J. Martin, Oncogene 29 (2010) 6428–6441, https://doi.org/10.1038/onc.2010.380.
[5] S. Medici, M. Peana, V.M. Nurchi, J.I. Lachowicz, G. Crisponi, M.A. Zoroddu, Coord. Chem. Rev. 284 (2015) 329–350, https://doi.org/10.1016/j.ccr.2014.08.002.
[6] M. Frik, A. Martínez, B.T. Elie, O. Gonzalo, D. Ramírez de Mingo, M. Sanaú, R. Sánchez-Delgado, T. Sadhukha, S. Prabha, J.W. Ramos, I. Marzo, M. Contel, J. Med. Chem. 57 (2014) 9995–10012, https://doi.org/10.1021/jm5012337.
[7] V. Brabec, J. Pracharova, J. Stepankova, P.J. Sadler, J. Kasparkova, J. Inorg. Biochem. 160 (2016) 149–155, https://doi.org/10.1016/j.jinorgbio.2015.12.029.
[8] QingYou Mo, JunGang Deng, Yani Liu, GuiDong Huang, ZuoWen Li, Ping Yu, Yi Gou, Feng Yang, Eur. J. Med. Chem. 156 (2018) 368–380, https://doi.org/10.1016/j.ejmech.2018.07.022.
[9] G. Gomathi, R. Gopalakrishnan, Mater. Sci. Eng. C 64 (2016) 133–138, https://doi.org/10.1016/j.msec.2016.03.084.
[10] Y. Harinath, D.H.K. Reddy, B.N. Kumar, C.H. Apparao, K. Seshaiah, Spectrochim. Acta Mol. Biomol. Spectrosc. 101 (2013) 264–272, https://doi.org/10.1016/j.saa.2012.09.085.
[11] A. Mahal, R.A.E. Halawa, S.A. Zabin, M. Ibrahim, M.A. Refai, T. Kaimari, World J. Org. Chem. 3 (2015) 1–8, https://doi.org/10.12691/wjoc-3-1-1.
[12] P. Dandawate, K. Vemuri, E.M. Khan, M. Sritharan, S. Padhye, Carbohydr. Polym. 108 (2014) 135–144, https://doi.org/10.1016/j.carbpol.2014.03.006.
[13] M.A. Abdelgawad, M.B. Labib, M.A. Latif, Bioorg. Chem. 74 (2017) 212–220, https://doi.org/10.1016/j.bioorg.2017.08.014.
[14] J.G. Deng, Y. Gou, W. Chen, X. Fu, H. Deng Bioorg, Med. Chem. 24 (2016) 2190–2198, https://doi.org/10.1016/j.bmc.2016.03.033.
[15] Zafar Iqbal, Shahid Hameed, Sher Ali, Tehseen Yildiz, Mohammad Shahid, Jamshed Iqbal, Eur. J. Med. Chem. 98 (2015) 127–138, https://doi.org/10.1016/j.ejmech.2015.05.011.
[16] Hyun-Jung Lee, Jin Sung Kim, Myung-Eun Suh, Hyen Joo Park, Sang Kook Lee, Hee-Kyung Rhee, Hwa Jung Kim, Eun-Kyung Seo, Choonmi Kim, Chong-Ock Lee, Hea-Young Park Choo, Eur. J. Med. Chem. 42 (2007) 168–174, https://doi.org/10.1016/j.ejmech.2015.05.011.
[17] Mahantesh Kumbar, Sangamesh A. Patil, Shivashankar S. Toragalmath, Shailaja S. Jawoor, Arun Shettar, Inorg. Chim. Acta. 500 (2020), 119210, https://doi.org/10.1016/j.ica.2019.119210.
[18] Mahantesh Kumbar, Sangamesh A. Patil, Shivashankar M. Kinnal, Shailaja S. Jawoor, Arun Shettar, Chem. Data Collect. 21 (2019), 100226, https://doi.org/10.1016/j.cdc.2019.100226.
[19] Sangamesh A. Patil, Vinod H. Naik, Ajaykumar D. Kulkarni, Udaykumar Kamble, Gangadhar B. Bagihalli, Prema S. Badami, J. Coord. Chem. 63 (2010) 688–699, https://doi.org/10.1080/00958971003602269.
[20] William G. DeGraff James Carmichael, Adi F. Gazdar, John D. Minna, James B. Mitchell, Canc. Res. 47 (1987) 936–942.
[21] Dominic A. Scudiero, Robert H. Shoemaker, Kenneth D. Paull, Anne Monks, Siobhan Tierney, Thomas H. Nofziger, Michael J. Currens, Donna Seniff, Michael R. Boyd, Canc. Res. 48 (1988) 4827–4833.
[22] M.A. Neelakantan, F. Rusalraj, J. Dharmaraja, S. Johnsonraja, T. Jeyakumar, M. Sankaranarayana Pillai, Spectrochim. Acta Mol. Biomol. Spectrosc. 71 (2008) 1599–1609, https://doi.org/10.1016/j.saa.2008.06.008.
[23] Chetan T. Prabhakara, Sangamesh A. Patil, Shivakumar S. Toragalmath, Shivashankar M. Kinnal, Prema S. Badami, J. Photochem. Photobiol. B Biol. 157 (2016) 1–14, https://doi.org/10.1016/j.jphotobiol.2016.02.004.
[24] Oleg Trott, J. Arthur, Olson, J. Comput. Chem. 31 (2010) 455–461, https://doi.org/10.1002/jcc.21334.
[25] A. Marin, N. Valls, F.J. Berenguer, M.T. Alonso, A. Ramon Martinez, M. Mercedes Martinez, J. Elguero, Farmaco 47 (1992) 63–75.
[26] Catherine A. Rice-Evans, Nicholas J. Miller, Paganga George, Trends Plant Sci. 2 (1997) 152–159.
[27] K. Nakamoto, Infrared and Raman Spectra of Inorganic and Coordination Compounds, fourth ed., John Wiley and Sons, 1986.
[28] G.B. Deacon, R.J. Phillips, Coord. Chem. Rev. 33 (1980) 227–250.
[29] Lekshmi V. Kumar, Rathika Nath, J. Chem. Sci. 131 (2019) 76, https://doi.org/10.1007/s12039-019-1658-x.
[30] Divya Hegde, Suneel Dodamani, Vijay Kumbar, Sunil Jalalpure, B. Kalagouda, Gudasi. Appl. Organomet. Chem. 31 (2017), e3851, https://doi.org/10.1002/aoc.3851.
[31] Sangamesh A. Patil, Chetan T. Prabhakara, Bhimashankar M. Halasangi, Shivakumar S. Toragalmath, Prema S. Badami, Spectrochim. Acta Mol. Biomol. Spectrosc. 137 (2015) 641–651, https://doi.org/10.1016/j.saa.2014.08.028.
[32] Donald L. Pavia, Gary M. Lampman and George S. Kriz. Introduction to Spectroscopy third ed. Brooks/Cole Thomson Learning.
[33] Edmond de Hoffmann, Stroobant Vincent, Mass Spectrometry, Principles and Applications, third ed., John Wiley and Sons, 2013.
[34] Jurgen H. Gross, Mass Spectrometry, A Textbook, second ed., Springer Publications, 2010.
[35] Geeta H. Chimmalagi, Umashri Kendur, Sunil M. Patil, Christopher S. Frampton, Kalagouda B. Gudasi, Delicia A. Barretto, Chandrashekhar V. Mangannavar, Iranna S. Muchchandi, Appl. Organomet. Chem. 33 (2019) e4557, https://doi.org/10.1002/aoc.4557.
[36] Luciano Antolini, Ledi Menabue, Gian C. Pellacani, Monica Saladini, Luigi P. Battaglia, Anna B. Corradi and giuseppe marcotrigian, J. Chem. Soc. Dalton Trans. 10 (1984) 2325–2326, https://doi.org/10.1039/DT9840002325.
[37] Sanjoy Saha, Goutam Basak, Biswajit Sinha, J. Chem. Sci. 130 (2018) 9, https://doi.org/10.1007/s12039-017-1409-9.
[38] M. Charles, Earnest. *Compositional Analysis By Thermogravimetry*, ASTM International, 1988.
[39] W.J. Geary, Coord. Chem. Rev. 7 (1971) 81–122.
[40] Qing Yang, Peng Yang, Xuhong Qian, Lianpeng Tong, Bioorg. Med. Chem. Lett 18 (2008) 6210–6213, https://doi.org/10.1016/j.bmcl.2008.09.104.

[41] Amani S. Alturiqi, Abdel-Nasser M.A. Alaghaz, Reda A. Ammar, Mohamed E. Zayed, J. Chem. 1–17 (2018) (2018), https://doi.org/10.1155/2018/5816906. Article ID: 5816906.
[42] Jing Zhang, Christophe Rouillon, Melina Kerou, Judith Reeks, Brugger Kim, Shirley Graham, Julia Reimann, Giuseppe Cannone, Huanting Liu, Sonja-Verena Albers, James H. Naismith, Laura Spagnolo, Malcolm F. White, Mol. Cell. 45 (2012) 303–313, https://doi.org/10.1016/j.molcel.2011.12.013.
[43] Chetan T. Prabhakara, Sangamesh A. Patil, Ajaykumar D. Kulkarni, Vinod H. Naik, M. Manjunatha, Shivashankar M. Kinnal, Prema S. Badami, J. Photochem. Photobiol. B Biol. 148 (2015) 322–332, https://doi.org/10.1016/j.jphotobiol.2015.03.033.
[44] Ibrahim Elghamry, Magdy M. Youssef, A Al-Omair Mohammed, Hany Elsawy, Eur. J. Med. Chem. 139 (2017) 107–113, https://doi.org/10.1016/j.ejmech.2017.07.079.
[45] Gangadhar B. Bagihalli, Sangamesh A. Patil, J. Coord. Chem. 62 (2009) 1690–1700, https://doi.org/10.1080/00958970802668851.
[46] J.C. Reed, Am. J. Pathol. 157 (2000) 1415–1430, https://doi.org/10.1016/S0002-9440(10)64779-7.
[47] Ikechukwu P. Ejidike, Peter A. Ajibade, Rev. Inorg. Chem. 35 (2015) 191–224, https://doi.org/10.1515/revic-2015-0007.